reflux ratio distilling head. Between the Corad head and the top of the column, a feed line from a constant flow bellows pump was introduced. The column had been calibrated with a test mixture of ethylbenzene and p-xylene, whose mixture possesses a relative volatility of 1.06. The column calibrated 4.5 theoretical plates at total reflux. A run was made with a charge comprising approximately 10% methylcyclohexane and 90% toluene in the stillpot. The column was operated at total reflux for about an hour and then the pump started at a rate to deliver about one part of extractive agent to one part of methylcyclohexane—toluene being boiled up. The extractive agent in this example was 33.3% phthalic anhydride, 33.3% maleic anhydride, and 33.3% glycerol triacetate. The following data were obtained:

Time, hours	Overhead Composition, % MCH,	% Tol.	Stillpot Composition, % MCH,	% Tol.	Relative Volatility
1	88.7	11.3	6.4	93.6	2.87
2	97.0	3.0	5.3	94.7	4.11
3	97.8	2.2	4.9	95.1	4.48

It will be noted that after about two hours, equilibrium has been achieved and the relative volatility remains essentially constant in the range 4.1 to 4.5. Without the extractive agent it would have been 1.50.

LITERATURE CITED

Atlani, M., V. Corso, and C. Wakselman, "Separation of Dienic, Naphthenic and Aromatic Hydrocarbons from Cuts Containing Them Using Cyanamide Solvents," Fr. Pat. 2,335,584 (Dec. 19, 1975).

Butler, R. M., and J. A. Bichard, "Separation of Aromatics from Hydrocarbon Streams," U.S. Pat. 3,114,783 (Dec. 17, 1963).

Cooper, H. B. H., and E. C. Medcalf, "Saturated Hydrocarbons by Extractive Distillation," U.S. Pat. 2,655,467 (Oct. 20, 1953).

Dunn, C. L., R. W. Millar, G. J. Pierotti, and R. N. Shiras, "Toluene Recovery by Extractive Distillation," *Trans. AIChE*, **41**, 631 (1945).

Eisenlohr, K., and H. Mueller, "Obtaining Pure Aromatics from Hydrocarbon Mixtures by Extractive Distillation," Ger. Pat. 2,263,344 (Dec. 23, 1972).

Mikitenko, P., G. Cohen, and L. Asselinieau, "Purification of Benzene & Toluene by Azeotropic Extractive Distillation," Ger. Pat. 2,313,603 (Sept. 27, 1973).

——— and L. Asselinieau, "Purification of Benzene & Toluene by Azeotropic-Extractive Distillation," Ger. Pat. 2,809,985 (Sept. 14, 1978).

Mueller, E., and K. P. John, "Separation of Pure Aromatic Hydrocarbons from Hydrocarbon Mixtures by Extractive Distillation," Ger. Pat. 1,808.758 (June 25, 1970).

Preusser, G., K. Richter, and M. Schulze, "Separating Aromatics from Hydrocarbon Mixtures by Extractive Distillation," Ger. Pat. 2,014,262 (Oct. 14, 1971).

Snyder, L. R., "Classification of the Solvent Properties of Common Liquids," *J. Chromat. Sci.*, **16**, 223 (1978).

Thompson, H. L., "Process for the Extraction & Recovery of Aromatic Hydrocarbons," U.S. Pat. 3,537,984 (Nov. 3, 1970).

——— "Aromatic Hydrocarbon Recovery by Extractive Distillation, Extraction & Plural Distillations, U.S. Pat. 3,723,256 (Mar. 27, 1973a).

——— "Extractive Distillation of Aromatic Hydrocarbons," Ger. Pat. 2,225,994 (Dec. 13, 1973b).

——— "Extractive Distillation of Hydrocarbons," Can. Pat. 962,212 (Feb. 4, 1975a).

——— "Extractive Distillation," Brit. Pat. 1,392,735 (Apr. 30, 1975b).

Manuscript received October 5, 1982; revision received January 4, and accepted January 24, 1983.

Pore-Diffusion Model for Cyclic Separation: Temperature Swing Separation of Hydrogen and Methane at Elevated Pressures

A pore-diffusion model is developed for temperature swing separation in a packed bed of sorbent. The model is applied to interpret experimental data for separation of H_2 of CH_4 in a packed bed of activated carbon operated in the temperature swing mode, at pressures up to 5.52 MPa. Experimental results on the effects of total pressure, particle size, adsorption temperature, and flow rate on separation efficiency compared favorably to the model predictions. The importance of pore diffusion in separation has been clearly demonstrated.

M. C. TSAI, S. S. WANG and R. T. YANG

Department of Chemical Engineering
State University of New York at Buffalo
Amherst, NY 14260

SCOPE

There is an increasing number of important industrial applications being found for temperature and pressure swing separation processes. Designs and performance models have been made and illustrated with various examples (Pigford et al., 1969, 1971; Kadlec et al., 1972, 1973; Wankat et al., 1975, 1978; Hill et al., 1980, 1982). In these models it has been assumed that the adsorbed phase is in instantaneous equilibrium with the bulk flow phase of the fluid. More specifically, in the model for temperature swing separation by Baker and Pigford (1971), pore diffusion is assumed instantaneous and a linear or Freundlich equilibrium adsorption isotherm is assumed. The first objective of this work is to formulate a more general model which incorporates pore diffusion limitation and Langmuir isotherm, the latter being more applicable for gases. Experimental results are also presented for separation of H_2 and CH_4 at elevated pressures using temperature swing in a packed bed of activated carbon.

Correspondence concerning this paper should be addressed to R. T. Yang.

CONCLUSIONS AND SIGNIFICANCE

The comparison between experimental results and the pore diffusion model showed that pore-diffusion limitation is important in modeling of temperature swing separation processes. Effective separation of H_2 and CH_4 can be achieved in a packed bed of activated carbon. It is shown in this study that pore diffusivity is a factor as important as contact time and equilibrium amounts adsorbed in determining separation efficiency. Changing a single operating variable usually involves changes of all three factors. It is shown that the net effects of these changes can only be predicted by the pore-diffusion model.

The pore-diffusion model is also useful in separation systems involving smaller diffusion coefficients, such as liquid and/or molecular sieve sorbents. Furthermore, it is pointed out that the pore-diffusion model may be used in selecting sorbent, such as the type of activated carbon, for a specific system. Equilibrium amounts of adsorption alone cannot fulfill this purpose.

INTRODUCTION

The separation of hydrogen from methane and other light hydrocarbons has been commercially practiced in the petroleum-refining industry and steam reforming of CH_4 for manufacturing ammonia, syngas and other chemicals. In these processes, a rather high purity of H_2 is required. For example, a purity of over 99% is necessary for most syngas-manufacturing processes. The prevalent separation process for these applications are based on cryogenic separation. The separation of hydrogen from methane is also an important step in advanced coal gasification and liquefaction processes. In these processes, however, a high purity of hydrogen or methane is not required. The methane content need only be enriched to about 90% to reach a heating value of 33.5 MJ/m^3, which would be sufficiently high for industrial and residential applications. The modern cryogenic processes may certainly be applied; however, here is clearly an opportunity for looking into other processes for such improvements as in lowering the energy requirements and increasing the throughput.

Theoretical treatment of the temperature-swing process was first made by Pigford et al. (1969, 1971). In this type of process, a fixed bed of sorbent is subject to cyclic heating and cooling at a frequency related to the capacity of adsorption. With a proper cycling frequency, the bed takes up the sorbate from the feedstream during the cooling half cycle and releases it during the heating half cycle. Thus, the effluent stream alternates between being leaner and richer in sorbate than that of the feed. Diverting the effluent to different receivers at appropriate times gives a semicontinuous flow of sorbate-enriched and sorbate-depleted products. Furthermore, the separation factor can be improved if the fluid flows through a sequence of beds which are cycled in temperature out of phase with each other (hot-cold-hot-cold . . .). As the sorbate-enriched portion of the effluent from bed 1 (hot) flows through bed 2 (cold), bed 2 is heated to release the adsorbed sorbate thus further enriching the already once enriched stream. This process repeats itself in the successive beds and achieves higher separation (Wankat et al., 1975, 1978).

In the previous models for predicting the performance of temperature swing separation processes (Pigford et al., 1971; Hill et al., 1982), the adsorbed and fluid phases are assumed to be in equilibrium, and pore diffusion and heat transfer are instantaneous. Also, a linear or Freundlich isotherm is used for equilibrium adsorption. However, for some industrially important processes, such as the separation of H_2 and CH_4 under pressure in a packed-bed column, these assumptions are not valid. In this paper, a more general model with the inclusion of the pore diffusion step is developed. The pore-diffusion model has been found applicable for predicting the performance of our separation system operated in the temperature swing mode.

The present model is basically a modified hybrid between the Pigford-Baker model (1971) and the isothermal model with pore diffusion by Masamune and Smith (1964). Mass balances of CH_4 are made for bulk flow in the packed-bed column and diffusion in the pores of a single particle. These two mass balance equations are coupled by the mass flux equation at the exterior surface of the particles. Numerical method is used to obtain solutions for these equations. The concentration of methane in the effluent stream from the packed bed can be predicted as a function of time for both heating half cycle and cooling half cycle. The main operating parameters involved in this study are total pressure, particle size, temperature, and product flow rate. Their effects on the effluent concentration of CH_4 are computed and compared with our experimental data.

PORE-DIFFUSION MODEL FOR CYCLIC SEPARATION

To simplify the derivation and calculation, the following assumptions and approximations are made:

1. Ideal gas law applies. (The compressibility factor for the gas mixture was calculated to be 0.99 under our experimental condition of 34 atm and 25°C.)
2. The axial pressure gradient across the bed is neglected.
3. Plug-flow condition holds; i.e., longitudinal dispersion along the bed is neglected.
4. Inside the pores, instantaneous equilibrium exists between the gas phase and the adsorbed phase.
5. Adsorption isotherm for CH_4 from single gas is used. The adsorption of H_2 from the mixture is neglected.
6. The mixture is assumed to vary uniformly in the bed, and temperature is equilibrated instantaneously between gas and solid.

Mass balances for both components CH_4(A) and H_2(B) in the packed-bed column at system pressure, P, and temperature, T, are given by:

$$\alpha \frac{\partial C_A}{\partial t} + \frac{\partial u C_A}{\partial z} - S = 0 \tag{1}$$

and

$$\alpha \frac{\partial C_B}{\partial t} + \frac{\partial u C_B}{\partial z} = 0 \tag{2}$$

where C_A and C_B are the concentrations of CH_4 and H_2, respectively, in bulk flow, and α is the interparticle void fraction. The velocity u is the superficial velocity, i.e., volumetric flow rate through a unit cross-sectional area of the column. The quantity S is the overall sorption rate of CH_4 per unit volume of bed. At a specific time when P is constant and T is nearly constant in a time interval (small enough), Eqs. 1 and 2 can be rewritten in terms of mole fractions, y_i, and become:

$$\alpha \frac{\partial y_A}{\partial t} + u \frac{\partial y_A}{\partial z} + y_A \frac{\partial u}{\partial z} - S \frac{RT}{P} = 0 \tag{3}$$

and

$$\alpha \frac{\partial y_B}{\partial t} + u \frac{\partial y_B}{\partial z} + y_B \frac{\partial u}{\partial z} = 0 \tag{4}$$

Since $y_B = 1 - y_A$, Eq. 4 becomes:

$$-\alpha \frac{\partial y_A}{\partial t} - u \frac{\partial y_A}{\partial z} + (1 - y_A) \frac{\partial u}{\partial z} = 0 \tag{5}$$

By combining Eqs. 3 and 5, the following equation is obtained for velocity gradient in the packed bed:

$$\frac{\partial u}{\partial z} = \frac{S}{P/RT} \tag{6}$$

If the velocity at one end of the bed and the values of S between this end and a specific location are known, one can calculate the velocity at this location. (See Appendix for detailed algorithm.) By inserting Eq. 6 into Eq. 3, the final equation is derived:

$$\alpha \frac{\partial y_A}{\partial t} + u \frac{\partial y_A}{\partial z} - (1 - y_A) \frac{SRT}{P} = 0 \tag{7}$$

Under the assumption that the bed is composed of spherical particles of uniform radius, a and that the net molar flux of H_2 is zero, the quantity S is the total molar flow of CH_4, N_{Ar}, through the exterior surfaces of the particles in a unit volume of bed:

$$S = + \frac{3\rho_B}{\rho_P}\left[\frac{1}{a}\right] N_{Ar}|_{r=a}$$
$$= -\frac{3\rho_B}{\rho_P}\left[\frac{D_e P}{aRT}\right]\left[\frac{1}{1 - y_A^*}\frac{\partial y_A^*}{\partial r}\right]_{r=a} \tag{8}$$

in which ρ_B and ρ_P are the densities of bed and particle, respectively. D_e is the effective diffusivity of CH_4 in the pores. The mole fraction of CH_4 inside the pores is denoted as y_A^*, which is a function of radial location r in the particle, time t, and axial location z along the column.

The external mass transfer resistance is neglected in this study for reasons described below. The simple criterion of Weisz and Hicks for evaluating the importance of external mass transfer cannot be used here because no surface reaction occurs. However, the following calculation should give a reliable order-of-magnitude estimate of its importance relative to internal pore diffusion. The mass flux across the external gas film is equal to the flux at the pore mouth inside the particle, or

$$k_g(y - y_s)C_t = D_e\left(\frac{dy^*}{dr}\right)_{r=a} C_t \tag{9}$$

where k_g is the mass transfer coefficient in the gas film, y is the bulk concentration, y_s is the surface value, and C_t is the total molar concentration and is equal on both sides. Now it is desired to evaluate $y - y_s$ and compare this value with the gradient inside the particle. The gas film resistance would be indeed negligible if this ratio is small. For the worst case, the value of k_g can be calculated for stokes regime where Sherwood number = 2, which gives the lowest k_g value. Using the particle diameter and gas diffusivity values, $k_g = 0.1$ cm/s. For the flux at the pore mouth inside the particle, the worst case is where and when the flux is the highest. This would be curve A (small time) for a particle at the entrance of the column (Figure 4 and later figures). Here, $D_e = 5 \times 10^{-7}$ cm^2/s and (dy^*/dr) at $r = a$ is 5 cm^{-1}. Using these worst cases, the ratio of Δy across the film over the Δy^* in the particle is approximately 10^{-4}. It is, therefore, clear that the external mass transfer resistance is negligible compared to pore diffusion in all cases.

The mass balance of CH_4 in the pores of a spherical particle at axial location z is given by

$$\epsilon \frac{\partial C_A^*}{\partial t} + \rho_P \frac{\partial q}{\partial t} + \frac{1}{r^2}\frac{\partial}{\partial r}(r^2 N_{Ar}) = 0 \tag{10}$$

where ϵ is the intraparticle void fraction, C_A^* is the concentration of CH_4 inside the pores. The quantity q is the number of moles of CH_4 adsorbed per gram of solid, and is a function of temperature T, total pressure P, and mole fraction y_A^*, that is $q = q(T,P,y_A^*)$. Therefore, Eq. 10 becomes

$$\frac{D_e}{1 - y_A^*}\left(\frac{\partial^2 y_A^*}{\partial r^2} + \frac{1}{1 - y_A^*}\left(\frac{\partial y_A^*}{\partial r}\right)^2 + \frac{2}{r}\frac{\partial y_A^*}{\partial r}\right) = \epsilon \frac{\partial y_A^*}{\partial t}$$
$$+ \rho_P \frac{RT}{P}\frac{\partial q}{\partial t} = \left(\epsilon + \rho_P \frac{RT}{P}\frac{\partial q}{\partial y_A^*}\right)\frac{\partial y_A^*}{\partial t}$$
$$+ \left(\rho_p \frac{RT}{P}\frac{\partial q}{\partial T}\right)\frac{\partial T}{\partial t} + \left(\rho_p \frac{RT}{P}\frac{\partial q}{\partial P}\right)\frac{\partial P}{\partial t} \tag{11}$$

The last term in Eq. 11 will be neglected in our numerical solution, because the system pressure is kept constant in our experiments. The second term from the last is kept, because $\rho_P \cdot \partial q/\partial T$ is large even though $\partial T/\partial t$ is very small.

It should be noted that, when writing Eqs. 1 and 2 in terms of mole fractions, a term involving the derivative of temperature with respect to time has been omitted. By including such a term, Eq. 6 can be rewritten as

$$\frac{\partial u}{\partial z} = \frac{S}{P/RT} + \frac{\alpha}{T}\frac{\partial T}{\partial t} \tag{6a}$$

In the following, we will comment on the effect of including this term on the final solution.

In all our experiments, the velocity was measured at the exit end of the packed bed and the velocity along the bed was computed by integrating Eq. 6 as shown in the Appendix. By including the additional term, namely $\alpha/T\ \partial T/\partial t$, the velocity gradient along the bed is increased and thus the velocity at all points along the bed will be lower. A lower velocity along the bed would result in better separation and a higher CH_4 concentration at the exit. By making an order of magnitude analysis, it is seen that the term $\alpha/T\ \partial T/\partial t$ is significant only at temperatures below 70°C. Thus, the effect of omitting the $\partial T/\partial t$ term will not change the final solution significantly.

To solve Eqs. 7, 8 and 11 for a heating or cooling half-cycle, the following initial and boundary conditions apply: In the backed bed,

$$t = 0, z > 0$$
$$y_A = y_{in}\ (= 0.50) \tag{12}$$
$$t > 0, z = 0$$
$$y_A = y_{in}\ (= 0.50) \tag{13}$$
$$t > 0, z = L, \frac{\partial y_A}{\partial z} = 0 \tag{13a}$$

In the pores,

$$t = 0, r > 0, y_A^*\ (= 0.50) \tag{14}$$
$$t > 0, \quad r = 0, \quad \frac{\partial y_A^*}{\partial r} = 0 \tag{15}$$
$$r = a, \quad y_A^* = y_A(t,z) \tag{16}$$

ADSORPTION ISOTHERM

The adsorption isotherms were measured manometrically in a separate static system at temperatures from 295 to 480 K and pressures up to 6.89 MPa (Saunders, 1982). The data of CH_4 isotherms were fitted to the Langmuir isotherm (Eq. 17) and can be represented by the following equations

$$\frac{V}{Vm} = \frac{Bp}{1 + Bp} \tag{17}$$
$$Vm = \frac{4.02 \times 10^4}{T}\ (\text{cm}^3\ \text{STP/g carbon}) \tag{18}$$
$$B = 5.51 \times 10^{-9} \exp\left(\frac{14.4 \times 10^3}{8.31 \times T}\right) \tag{19}$$

Here, V is the volume adsorbed in cm^3 STP per gram of carbon at pressure p (in Pa) and temperature T (in K), and Vm is the volume corresponding to monolayer coverage. B is a constant related to the net enthalpy, ΔH, of adsorption according to the Langmuir theory. It has been noted (Saunders, 1982) that the monolayer coverage decreases with increasing temperature because of the increaing molecular area, and that the ethalpy of adsorption (ΔH = 14.4 kJ/mol) is higher than the latent heat of condensation of CH_4 (7.95 kJ/mol at its critical temperature of 191 K). Equations 17 to 19 to be substituted into Eq. 11 where V is related to the quantity q in Eq. 4 by dividing the factor of 22.4×10^3, and p is related to Py_A^* by ideal gas law.

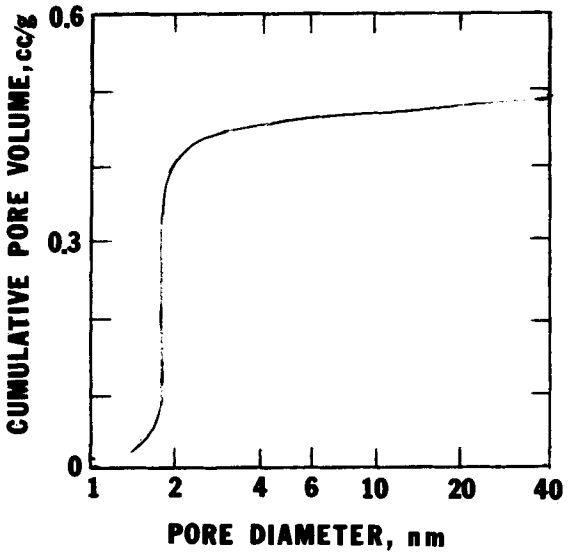

Figure 1. Pore-size distribution of PCB activated carbon.

TABLE 1. PHYSICAL PROPERTIES OF PCB ACTIVATED CARBON

Bulk Density, ρ_b	0.44 g/cm^3
Particle Density, ρ_p	0.85 g/cm^3
True Solid Density, ρ_t	2.2 g/cm^3
Interparticle Void Fraction in Packed Bed, α	0.48
Intraparticle Void Fraction, ϵ	0.61

METHOD OF SOLUTION

To formulate a numerical solution for Eqs. 7, 8 and 11, the packed bed is considered to be composed of ten cells, in each of which the molar fraction is homogeneous. Each particle in the ith cell is divided into five shells, and the molar fraction in each shell is also considered homogeneous.

Crank-Nicolson method is used to solve Eq. 7, and is both stable and convergent for a wide range of parameter values investigated. However, because of the complexity of Eq. 11, explicit (or direct) method is used. Therefore, a sufficiently small time step (Δt) is chosen to achieve both stability and convergence of the solution. The simple numerical differentiation method is used for Eq. 8. Also, to correct for the temperature and pressure changes, the following approximations are made for effective diffusivity at each time step $j\Delta t$:

$$D_{e_j} = D_{e_o}\left[\frac{T_j}{T_o}\right]^a\left[\frac{P_o}{P_j}\right]^b; \quad \text{where } a = 1, \quad b = 1 \qquad (20)$$

Although the temperature dependence ranges from $T^{0.5}$ (for Knudsen diffusion) to $T^{1.75}$ (for molecular diffusion), the dependence for pore diffusion in the transition regime, especially for carbon, is linear (Yang and Liu, 1982). It should be noted that the pressure correction factor is not used in this work, because the system pressure is maintained constant.

EXPERIMENTAL

The separation of hydrogen-methane using activated carbon was studied in a continuous flow system with a packed-bed sorption column operating in a temperature-swing mode. Activated carbon (designated PCB) was supplied by Calgon Corp. The physical properties of PCB carbon are shown in Table 1, and the pore structure is shown in Figure 1.

Apparatus for Temperature-Swing Separation

Schematic diagram of the apparatus is shown in Figure 2. The flow system was designed to give a breakthrough time of the order of 30 minutes.

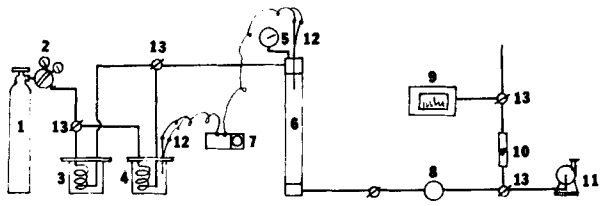

Figure 2. Schematic of apparatus for temperature swing separation: 1. Premixed feed gas, 2. regulator, 3. constant temperature bath, 4. fluidized-bed sand bath, 5. pressure gauge, 6. adsorption column, 7. temperature readout, 8. back pressure valve, 9. gas chromatograph, 10. rotameter, 11. pump, 12. thermocouple well, 13. three-way valve.

The inlet gas mixture of CH_4/H_2 (volume ratio 50/50) was a custom-made, premixed gas supplied by Linde Div. of Union Carbide. A water bath was used for precooling the inlet gas during the cooling half cycle. A fluidized-bed sand bath (Tecam, SBS-2) was used to preheat the inlet gas during the heating period. The sorption column with inside diameter 4.6 cm and external height 60 cm was packed with 40-cm height of carbon. The temperature of the bed was monitored with a thermocouple inserted into the bed about 10 cm below the bed surface, and was displayed on a digital readout (Omega, 2166A). The system pressure was monitored with a pressure gauge inserted above the bed surface. The pressure was controlled with a back-pressure valve downstream (below the bed). The effluent flow rate was controlled at a desired steady rate by adjusting the back-pressure valve and a needle valve. Besides preheating and precooling the feed gas mixture, additional heating of the column was provided by a heating tape surrounding the column. An insulation jacket was used during the heating cycle. During the cooling cycle, the insulation was taken off and four blowers were used to accelerate cooling of the column. The CH_4 content in the effluent stream was analyzed with a gas chromatograph (Gow-Mac, with thermal conductivity detector and a Porapak Q column) at time intervals of about 5 minutes.

The one-point measurement for bed temperature was adopted to simplify the experiments. However, it is important to have a knowledge of the temperature distributions within the bed and within the particle. An estimate of the magnitude of the temperature distribution in the bed was obtained by a calibration run in which the pressure was held at the ambient value (Wang, 1982). In this experiment, the temperatures at five locations in the bed (three longitudinal points at the center and two radial ones in the middle) were measured during temperature cycling and they showed a maximum spread of approximately 8 K. The spread was not excessively large because of the long cycle time (80 min). Multipoint temperature measurements under pressure are not possible with the present apparatus. Further comments concerning the temperature distribution are:

(1) Using the combined heat-transfer technique, i.e. by preheating (precooling) the feed gas and heating (cooling) the column wall, the bed temperature could be changed much more rapidly than what we actually did, which gave a cycle time of about 80 min. The slow cooling and heating, Figure 3, were deliberately controlled to achieve constant total column pressure and constant product flow rate.

(2) Because of the slow superficial velocity in the bed, the major contribution to heating and cooling of the bed was from the wall. The radial temperature distribution may be estimated by solving the transient heat conduction problem. Thus, by using the following values: $\rho_b = 0.44$ g/cm^3, $C_p = 1.05$ J/g/K and effective conductivity = 0.004 J/cm/s/K, the values of $(T_{average} - 298)/(T_{wall} - 298) = 0.7$ in 5 min and 0.9 in 10 min. The values of this parameter are much higher for a particle. The times required for a uniform temperature distribution within the bed and within the particle are thus much shorter than the actual cycle time used in the experiments. Based on the above observations and our preliminary calibration experiment, the temperature may be considered as uniform and the one-point measurement adequate.

Experimental Procedure

Before a typical experiment, the flow system was leak-tested and evacuated to 10 Pa. The system was subsequently pressurized to a desired system pressure with the feed gas mixture. The effluent flow was maintained at a constant flow rate by manipulating the regulator on the feed gas cylinder and the back pressure valve downstream. The effluent gas was sampled every 10 min to check the CH_4 concentration. When the CH_4 content in the effluent reached 50 (i.e., the column was saturated with CH_4), the heating half cycle followed. Both bed temperature and effluent concentration were recorded every 5 min. When the CH_4 concentration had passed a maximum and started leveling off to the feed concentration, the heating

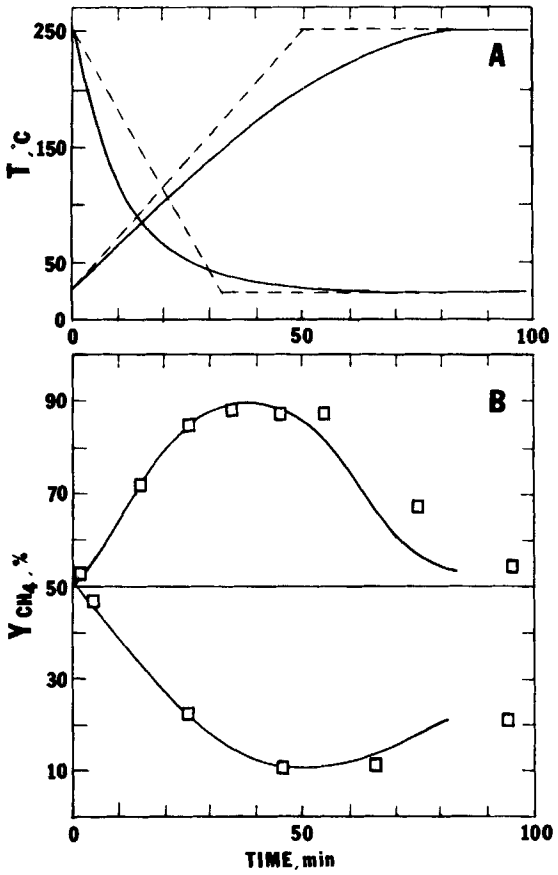

Figure 3. Temperature swing experiment. A. Temperature history: — exp., - - - - used in model. B. Concentration history: □ experimental data: — theoretical results.

TABLE 2. INPUT PARAMETERS FOR MODELING AS SHOWN IN FIGURE 3

	Heating Half Cycle	Cooling Half Cycle
Packed-Bed Length, L	40.0 cm	40.0 cm
Initial Temperature, T_o	298 K	523 K
Final Temperature, T_f	523 K	298 K
System Pressure, P	3.45 MPa	3.45 MPa
Heating or Cooling Rate, T_r	4.5 K/min	−7.0 K/min
Inlet Concentration of CH_4, y_{in}	0.50	0.50
Product Flow Rate (at STP), G	600 cm^3/min	200 cm^3/min
Particle Size, a	0.05 cm	0.05 cm
Effective Diffusivity at Initial Conditions, D_{e_o}	2.0×10^{-5} cm^2/min (3.3×10^{-7} cm^2/s)	6.0×10^{-5} cm^2/min (1.0×10^{-6} cm^2/s)

half cycle was completed. To start a cooling half cycle, the feed gas mixture was diverted through the water bath, and the power supply of the heating tape was turned off. The insulation jacket was removed from the column and the air blowers were switched on to cool the column. As in the heating interval, the effluent flow rate was maintained at the same level and the CH_4 concentration was recorded every 5 min. When the concentration had passed a minimum and returned to the feed concentration, the cooling half cycle was completed.

RESULTS AND DISCUSSION

Experiments on temperature-swing process were conducted with PCB activated carbon as the bed material. With a feed of 50/50 mixture of CH_4 and H_2, a 90/10 separation has been routinely achieved. Such a separation, when the products are collected semicontinuously, would be good enough for high-Btu gas production purposes. Typical experimental results and the corresponding mathematical modeling of the process are presented in Figure 3. Numerical values of the input parameters for the modeling are given in Table 2.

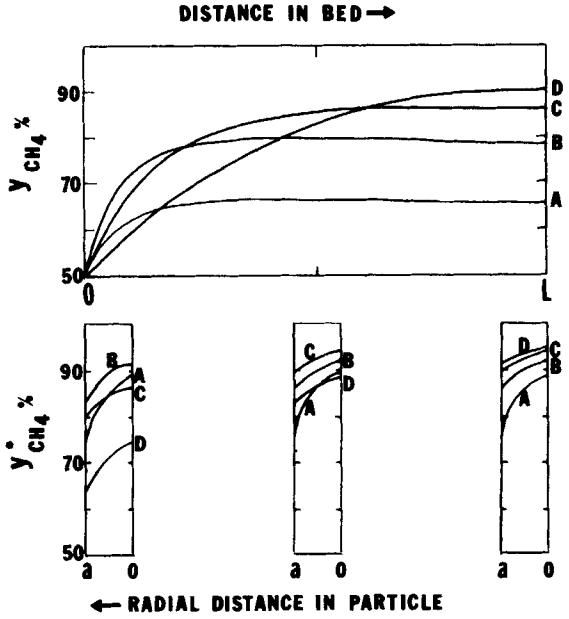

Figure 4. Concentration profiles in the heating half cycle in the packed bed and in particles at entrance, middle and exit points in the bed. (Input data are given in Table 2.) Time = 10 min (A), 20 min (B), 30 min (C) and 40 min (D).

The agreement between these results and the values predicted by the pore-diffusion model is fairly good except in the later stage of the half cycle. This discrepancy is caused by the difference between the actual temperature history and the assumed one used in the model (Figure 3). Also, a better approximate equation than Eq. 20 should also be helpful. The temperature histories were slightly different for the subsequent runs. But straight line profiles were used in modeling for all runs.

Figure 4 shows predicted concentration profiles in the packed bed and within a particle at three different locations, i.e., at entrance, middle and exit locations, during a heating half cycle. The profiles are plotted at various times. The input values in Table 2 were used in the model.

An explanation of the concentration profiles shown in Figure 4 and the subsequent figures is necessary at this point. In the numerical solution, the column is divided into ten cells and each particle is divided into five shells. The concentration in each shell or cell is uniform. The profiles shown in the figures were obtained by connecting the ten or five points with a smooth curve. Because only five shells were taken for the particle, there appeared to be some problems in the concentration profiles (of y^*), especially for a particle in the first cell of the column, or at the "entrance." The values of y^* at $r = a$ shown in the figures were the uniform concentrations in the first shell of the particle which was in the first cell. These values were not 50%. But the values of y^* in the zeroth shell were 50%, which are not shown in these figures. The y^* values declined rapidly to the y values beyond $r = a$. Also, at $r = 0$, the y^* values in the fifth shell may not appear to have a plateau in a few cases, but the gradient is zero at the center.

It was found that an effective diffusivity of 2×10^{-5} cm^2/min could best fit our experimental data, Figure 3. Figure 5 illustrates the influence of effective diffusivity. Higher values of D_e will improve the separation. However, when D_e is sufficiently high, there is no further improvement, and the performance is no longer limited by pore diffusion. Under our experimental conditions, Figure 5, it is predicted that for D_e greater than about 5×10^{-5} cm^2/min pore diffusion is no longer important. Establishment of a criterion for predicting the presence or absence of pore-diffusion limitation has not been successful.

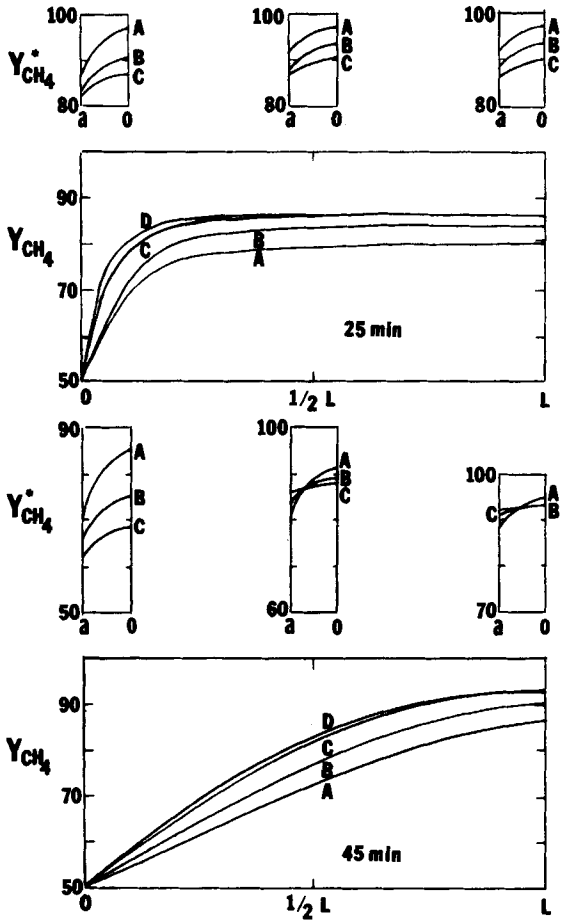

Figure 5. Effects of effective pore diffusivity on concentration profiles as predicted by model. A = 1×10^{-5}, B = 2×10^{-5}, C = 4×10^{-5} and D = 6×10^{-5} cm²/min for D_e. (Other conditions are given in Table 2.)

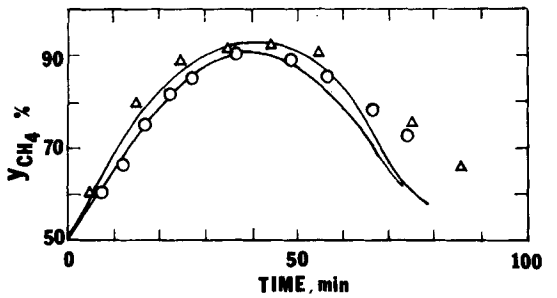

Figure 6. Effect of particle size on effluent concentration. For size 12/30 mesh: O experimental, — theoretical. For size 60/100 mesh: Δ experimental, — theoretical. (All other conditions are given in Table 2 and Figure 3.)

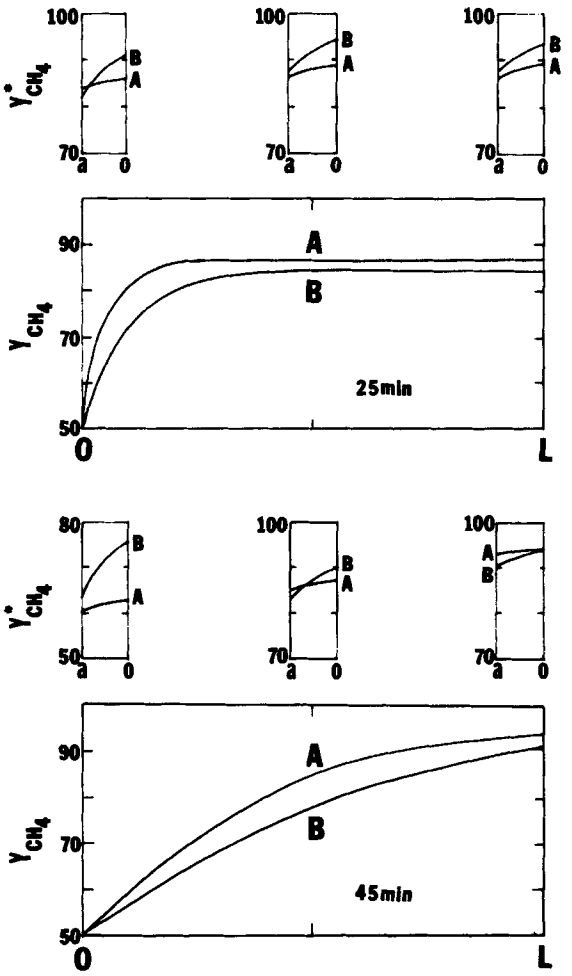

Figure 7. Effects of particle size on predicted concentration profiles. A = 0.02 cm and B = 0.05 cm radius. (Other parameters are the same as in Table 2.)

Effects of various operating parameters on the performance of temperature-swing separation have been examined experimentally and the results compared with predictions by the pore-diffusion model. The operating variables investigated were particle size, total pressure, flow rate, and the adsorption temperature. The following discussion is limited to heating half cycle, the results for cooling half cycle were similar to those for the heating half cycle and will not be shown here.

Effect of Particle Size

The study was limited to two-size fractions: 12–30 US mesh and 60–100 US mesh. The experimental data were compared with the predicted values, Figure 6. The maximum CH_4 effluent concentrations were 92% and 90% for 60/100 fraction and 12/30 fraction, respectively. The sorbent with the smaller-size fraction gave better separation and shorter cycling time, which are desirable. The discrepancy between experimental and theoretical results in the later stage was due to the lower experimental heating rate than the one used in the model. Figure 7 shows the effects of particle size on concentration profiles in the packed bed and within the particle. As expected, the profiles for larger particles are usually lower in the bed, but higher in the pores. When the particle size is sufficiently small, the pore-diffusion limitation will no longer be important. This point becomes clear when one compares the results for the small size fraction (in Figure 7) with the data in Figure 5.

Effect of Total Pressure

The effects of total pressure on separation are compared with model predictions, Figure 8. Under our experimental conditions, the most favorable pressure was 3.45 MPa. The least favorable results were 5.52 MPa where the CH_4 effluent concentrations were 87% for the hot half cycles. The product flow rates were kept constant. The use of equilibrium adsorption data as a guide in determining the pressure effect on separation would be clearly faulty. The fact that adsorption of CH_4 is stronger at a higher total pressure is obviously not reflected in the results. The crossover of the effluent concentrations for the two total pressures at about 50 min (Figure 8) is also predicted by the model (Figures 8 and 9). There are two opposing factors concerning the effect of total pressure: (1) A higher total pressure (at constant product rate) increases the contact time of the gas in the bed and consequently enhances the separation. (2) The effective pore diffusivity is lower at a higher pressure which

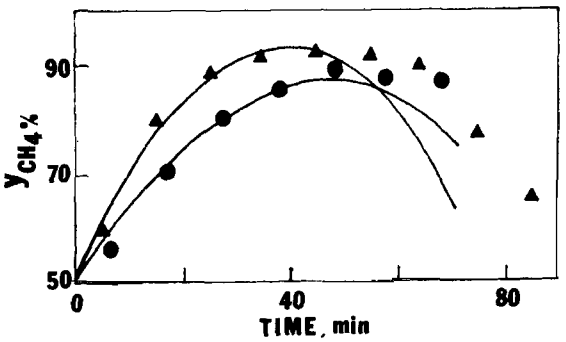

Figure 8. Effects of total pressure on effluent concentration. Particle size = 60/100 mesh. Total pressure = 3.45 MPa (▲), 5.52 MPa (●). Solid lines are theoretical values. (Other conditions are listed in Table 2.)

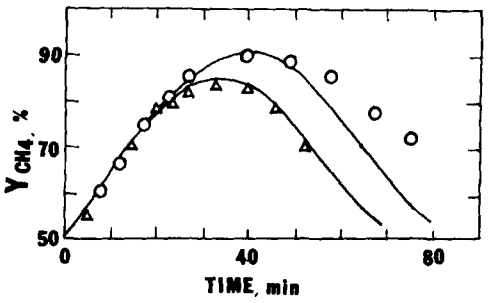

Figure 10. Effect of product flow rate on separation. Pressure = 3.45 MPa and size = 12/30 mesh. Flow rate = 600 (○) and 800 (△) cm³ STP/min. Solid lines are theoretical. (Other conditions are shown in Table 2.)

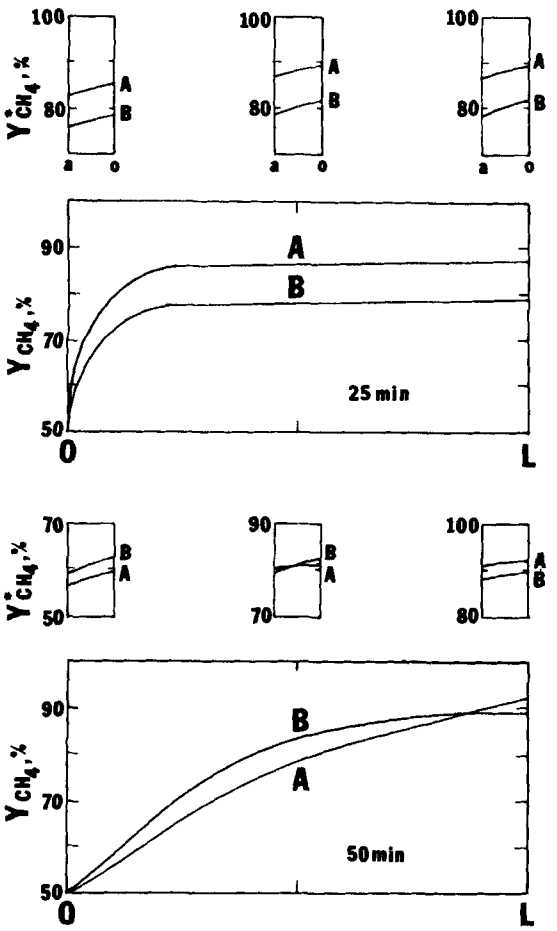

Figure 9. Effects of total pressure on predicted concentration profiles. A = 3.45 and B = 5.52 MPa. (Other conditions are shown in Table 2.)

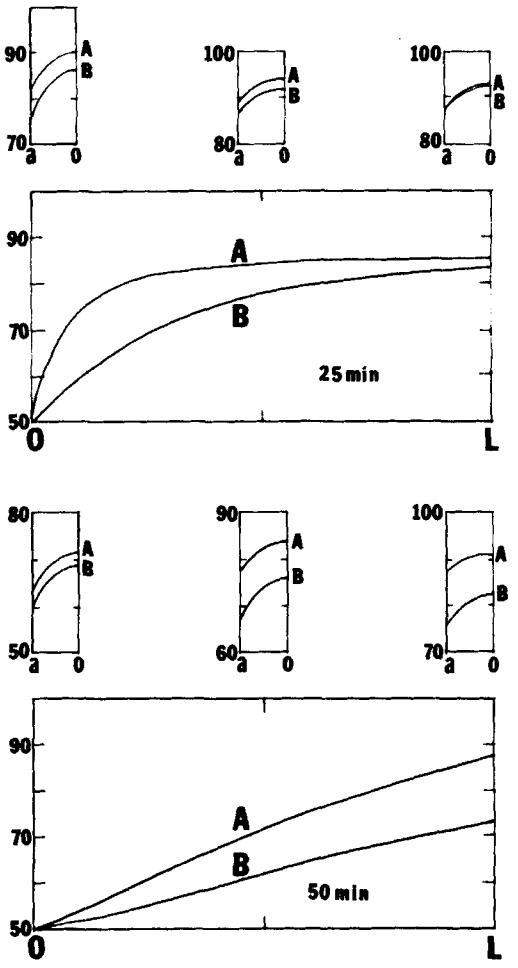

Figure 11. Effects of product flow rate on predicted concentration profiles. A = 600 and B = 800 cm³ STP/min. (Other conditions are shown in Table 2.)

reduces the separation efficiency. The net result of the two opposing factors can be predicted and understood through the pore-diffusion model.

Effect of Product Flow Rate

The effect of gas flow rate on performance was determined for two product flow rates: 600 and 800 cm³ (STP)/min, the other operating parameters were kept the same. The experimental data and corresponding theoretical results are shown in Figure 10. The highest effluent concentration was lowered from 90 to 83% with the flow rate increased from 600 to 800 cm³ (STP)/min. The trade-off of using a lower flow rate is that a lower rate gives higher separation factor at the cost of a longer half-cycle time. Figure 11 shows the theoretical predictions of the concentration profiles in the bed and in a particle at three positions along the bed at two times during the desorption half cycle.

The effect of bed height can also be predicted from Figure 11. Such an effect is similar to that of product flow rate.

Effect of Temperature Differential

The effect of ΔT was illustrated by changing the adsorption temperature, i.e., temperature of the cooling half cycle. The results for adsorption temperatures of 298 and 353 K (keeping the desorption temperature at 523 K) are shown in Figure 12. The results are predictable simply from equilibrium adsorption. In this case, the equilibrium adsorption of CH_4 was 1.26×10^3 mol/m³ of bed

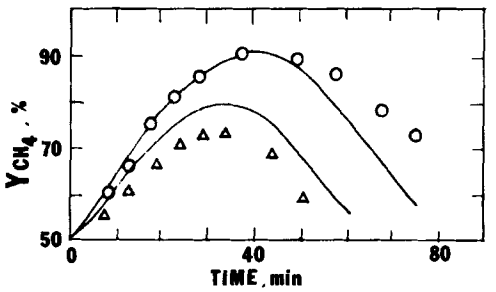

Figure 12. Effect of adsorption temperature on separation, at 3.45 MPa, 12/30 mesh size and 523 K desorption temperature. Adsorption temperature = 298 K (○) and 353 K (△). Solid lines are theoretical. (Other conditions are shown on Table 2.)

at 353 K; the value of 298 K was 2.17. The effect of D_e (pore diffusivity) appeared to be rather unimportant in this experiment, unlike the experiment on the effect of total pressure where D_e played an important role. In this experiment, D_e was higher in the initial period of desorption for the 353 K run. The effect of varying the desorption temperature, i.e., temperature of the hot half cycle, was not investigated. But such an effect would be less than that of the adsorption temperature, because the equilibrium amounts adsorbed are small at higher temperatures and hence the difference among them. The above discussion is clearly illustrated by the concentration profiles shown in Figure 13.

Pore Diffusivity in Activated Carbon

In the pore-diffusion model, the effective pore diffusivity is the only fitting parameter, which is determined by fitting the separation results with the model. The pore diffusivity varies with T and P according to Eq. 20. In addition, the values obtained here are overall values averaged over the entire bed because D_e varies with bed height.

The type of activated carbon used in this study is widely recommended by carbon manufacturers for gas separation and purification. The pore size of this carbon is predominantly in the range of 1.5 to 2.0 nm in diameter. The diffusing CH_4 molecule has a diameter of about 0.4 nm calculated from viscosity data at 293 K. It is expected that the pore diffusion would be quite restricted especially when there is a significant amount of surface coverage, when the dimensions of the free path are similar to that of CH_4. The interactions between the diffusing molecule and the adsorbed phase should be quite strong. Consequently, the D_e value should be dependent on the amount adsorbed, or the stage or time during heating or cooling half cycle. This explains the results of the D_e values of 3.3×10^{-7} cm^2/s at the start of the heating half cycle, and of 1.0×10^{-6} cm^2/s at the start of the cooling half cycle, for a total pressure of 3.45 MPa. The experimental pore diffusivity is thus increased by a factor of about 3 whereas the predicted ratio due to the temperature dependence (Eq. 20) is about 1.7 (the temperature being 298 and 523 K). The discrepancy is apparently caused by the adsorbed CH_4 at the start of the cooling half cycle.

The D_e values are about four orders of magnitude lower than the molecular diffusivities. This difference may be interpreted by the results obtained in the studies of "restricted diffusion." The following general expression has been used for restricted diffusion (Satterfield et al., 1973; Prasher and Ma, 1977):

$$D_e = \frac{D_g}{\tau} f(\lambda, K_p) \tag{21}$$

in which τ is the tortuosity factor, λ is the diameter ratio of molecule to pore, and K_p is the equilibrium partition coefficient. If we take the form suggested by Satterfield and Colton et al. (1973)

$$D_e = \frac{D_g}{\tau K_p} 10^{-2\lambda} \tag{22}$$

an order-of-magnitude analysis may be made as follows. The

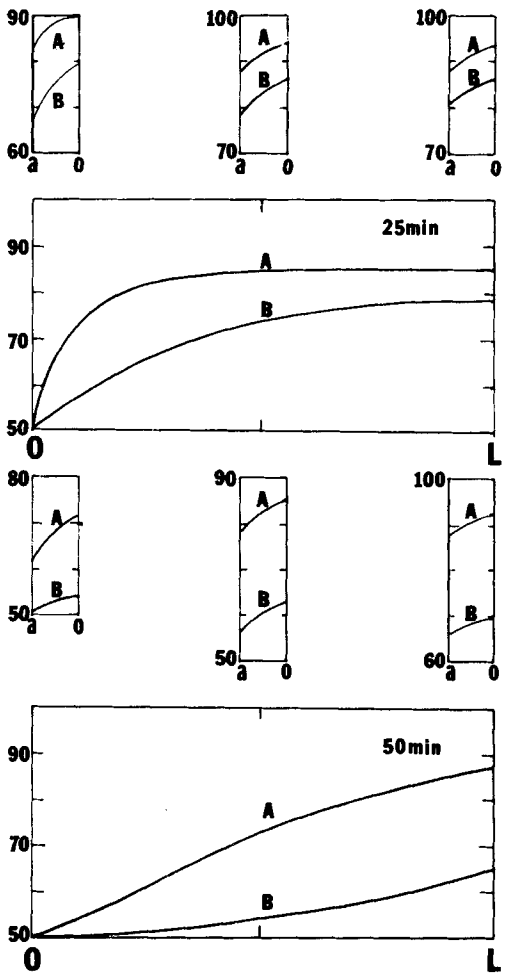

Figure 13. Effects of adsorption temperature on predicted concentration profiles. A = 298 K and B = 353 K for adsorption temperature. (Other conditions are the same as in Figure 12.)

equilibrium partition coefficient, which is the ratio of pore over bulk concentrations, is about 10 in our experiments. The restriction factor, $10^{-2\lambda}$, λ being the ratio of adsorbate and free pore diameters, may be taken as 10^{-1}. The tortuosity factor in carbon is quite high and has been determined to be of the order of 10^2 (Yang and Liu, 1982). The values of D_e calculated from the pore-diffusion model are, therefore, reasonable.

CONCLUDING REMARKS

Temperature-swing experiments have shown the feasibility of producing a high-Btu gas from a H_2/CH_4 mixture, e.g., from a coal gasifier. A pore-diffusion model is formulated which has been used successfully to predict the performance of the cyclic separation process and the effects of the operating variables.

It is shown in this study that pore diffusivity is a factor as important as contact time and equilibrium amounts adsorbed in determining the separation efficiency. Changing a single operating variable frequently involves changes in all three factors. The net effect can be predicted only by the pore-diffusion model. For example, by increasing the total pressure (keeping feed rate constant) the contact time and the equilibrium adsorption are increased (both favoring better separation), but the pore diffusivity is decreased and the net result is a lower separation efficiency, which is shown experimentally and predictable by the pore-diffusion model.

The pore-diffusion model should also be useful for liquid systems and processes involving molecular sieves where pore diffusion is more restrictive to separation. Furthermore, it is clear from the results of this study that the equilibrium adsorption alone cannot

be used as a guide for selecting adsorbent, but the pore-diffusion model should be used. It is noted that a similar but simplified model has been used for pressure swing adsorption, which is of more commercial interest, and the results will be reported shortly.

ACKNOWLEDGMENT

This work was supported by U.S. Department of Energy under Contract No. DE-AC21-80MC14386.

NOTATION

a = average radius of sorbent particle, cm
B = a constant related to the net enthalpy, ΔH, of adsorption according to Langmuir theory, MPa^{-1}
C = concentration of sorbate in bulk flow, mol/L
C_t = total molar concentration
C^* = concentration of sorbate inside the pores, mol/L
D_e = effective diffusivity of sorbate, cm^2/min or cm^2/s
D_g = molecular diffusivity, cm^2/s
k_g = mass transfer coefficient in the gas film
N_{Ar} = molar flux of CH_4 in radial direction
p = partial pressure of adsorbate, MPa
P = system pressure, MPa
q = number of moles of sorbate adsorbed per gram of solid, mol/g of solid
r = radial distance from center of spherical particle, cm
R = gas constant
S = overall rate of sorption per unit volume of bed, mol/L/min
t = time, min or s
T = solid or bed temperature, K
u = superficial velocity, cm/min
V = volume adsorbed per gram of sorbent, cm^3 (STP)/g of solid
Vm = volume corresponding to monolayer coverage, cm^3 (STP)/g of solid
y_i = mole fraction of species i
z = axial distance along the bed, cm

Greek Letters

α = interparticle void fraction
Δt = time step, min
ϵ = intraparticle void fraction
ρ_B = bed density, g/cm^3
ρ_P = particle density, g/cm^3
τ = tortuosity

Subscripts

A = CH_4
B = H_2
i = species, or cell or shell number
in = at inlet
j = time step
o = initial condition

Superscript

$*$ = inside the pores

APPENDIX

To calculate the velocity at a particular time step and location from Eq. 6, one boundary condition is needed. If the velocity at the exit end [the $(M+1)$th cell] is known, the velocity of gas mixture from the Mth cell is given by

$$u_M = u_{M+1} - \frac{S_{M+1}}{P/RT}\Delta z$$

where S_{M+1} is the sorption rate of CH_4 in the $(M+1)$th cell, and Δz is the length of the cell. Therefore, the velocity from the ith cell is

$$u_i = u_{M+1} - \frac{\Delta z}{P/RT}(S_{M+1} + S_M + \ldots + S_{i+1})$$

The numerical method used to solve Eq. 8 is based on the Crank-Nicolson method, which is a modification of the implicit finite difference method. The numerical formulation of Eq. 8 is as follows:

$$\alpha\frac{y_i' - y_i}{\Delta t} + \frac{u_i}{2\Delta z}\left[\frac{(y_{i+1}' - y_{i-1}') + (y_{i+1} - y_{i-1})}{2}\right] - \frac{S_i}{P/RT}(1 - y_i) = 0$$

By defining $A = u_i\Delta t/2\Delta z\alpha$ and $B = \Delta t/\alpha\, RT_i/P_i\, S_i$, the following equation is obtained

$$-\frac{1}{2}Ay_{i-1}' + y_i' + \frac{1}{2}Ay_{i+1}' = y_i + B(1 - y_i) - \frac{A}{2}(y_{i+1} - y_{i-1})$$

The superscript prime denotes a value at the end of a time step and the subscript i denotes the cell at a distance $i\Delta z$ in the direction of flow. For the first cell $(i = 2)$, we have

$$-\frac{1}{2}Ay_1' + y_2' + \frac{1}{2}Ay_3' = y_2(1 - B) + \frac{A}{2}(y_3 - y_1) + B$$

For the last cell $(i = M + 1)$,

$$-\frac{1}{2}Ay_M' + y_{M+1}' + \frac{1}{2}Ay_{M+2}' = y_{M+1}(1 - B) + \frac{A}{2}(y_{M+2} - y_M)$$

since $y_M' = y_{M+2}'$ and $y_M = y_{M+2}$, we have

$$y_{M+1}' = y_{M+1}(1 - B)$$

Gauss elimination method is used to solve this system of linear simultaneous equations having a tridiagonal coefficient matrix. To solve Eq. 11, we first define $R = a - r$, the equation becomes

$$\frac{1}{1 - y_A^*}\left(\frac{\partial^2 y_A^*}{\partial R^2} + \frac{1}{1 - y_A^*}\left(\frac{\partial y_A^*}{\partial R}\right)^2 - \frac{2}{a - R}\frac{\partial y_A^*}{\partial R}\right) = \frac{1}{D_e}\left(\epsilon + 1{,}000\,\rho_p\frac{RT}{P}\frac{\partial q}{\partial y_A^*}\right)\frac{\partial y_A^*}{\tau} + \left(1{,}000\,\frac{\rho_p}{D_e}\frac{RT}{P}\frac{\partial q}{\partial T}\right)\frac{\partial T}{\partial t}$$

The initial and boundary conditions become:

$$t = 0, \quad y_A^* = 0.50$$

$$R = a, \quad y_A^* = y_A$$

$$R = 0, \quad \frac{\partial y_A^*}{\partial R} = 0$$

Let $\psi = y_A^*$, $\beta = 1/D_e(\epsilon + 1{,}000\,\rho_p\, RT/P\,\partial q/\partial\psi)$, then the explicit finite difference formulation for this equation can be written as:

$$\psi_i' = \psi_i + \frac{1}{\beta}\frac{\Delta t}{(\Delta R)^2}\frac{\psi_{i-1} - 2\psi_i + \psi_{i+1}}{1 - \psi_i} + \frac{1}{\beta}\frac{\Delta t}{\Delta R^2}\frac{1}{4}\left(\frac{\psi_{i+1} - \psi_{i-1}}{1 - \psi_i}\right)^2 - \frac{1}{\beta}\frac{\Delta t}{(a - i\Delta R)\Delta R}\frac{\psi_{i+1} - \psi_{i-1}}{1 - \psi_i} - \frac{1}{\beta}\frac{\rho_p \times 1{,}000}{D_e}\frac{RT}{P}\frac{\partial q}{\partial T}\Delta T$$

This is a simple linear equation, which can be easily solved if the quantity q can be expressed as

$$q = \frac{B_1\psi}{1 + B_2\psi}, \quad \text{where } B_1 = \frac{K_5}{T}\exp\left(\frac{K_3}{T}\right), \quad B_2 = K_4\exp\left(\frac{K_3}{T}\right)$$

and K_3, K_4, K_5 are constants.

then

$$\left(\frac{\partial q}{\partial\psi}\right)_{T,P} = \frac{B_1}{(1 + B_2\psi)^2}$$

$$\left(\frac{\partial q}{\partial T}\right)_{P,\psi} = \frac{\psi B_1}{T(1 + B_2\psi)^2}\left[-\frac{K_3}{T} - 1 - \psi B_2\right]$$

LITERATURE CITED

Baker, III, B., and R. L. Pigford, "Cycling Zone Adsorption: Quantitative Theory and Experimental Results," *Ind. Eng. Chem. Fund.*, **10**, 283 (1971).

Hill, F. B., Y. W. Wong, and Y. N. I. Chan, "A Temperature Swing Process for Hydrogen Isotope Separation," *AIChE J.*, **28**, 1 (1982).

Kowler, D. E., and R. H. Kadlec, "The Optimal Control of a Periodic Adsorber," *ibid.*, **18**, 1207, 1212 (1972).

Masamune, S., and J. M. Smith, "Adsorption Rate Studies—Significance of Pore Diffusion," *ibid.*, **10**, 246 (1964).

Pigford, R. L., B. Baker, III, and D. E. Blum, "Cycling Zone Adsorption, a New Separation Process," *Ind. Eng. Chem. Fund.*, **8**, 848 (1969).

Prasher, B. D., and Y. H. Ma, "Liquid Diffusion in Microporous Alumina Pellets," *AIChE J.*, **23**, 303 (1977).

Satterfield, C. N., C. K. Colton, and W. H. Pitcher, Jr., "Restricted Diffusion in Liquids Within Fine Pores," *ibid.*, **19**, 628 (1973).

Saunders, J. T., "Adsorption of H_2/CH_4 Mixtures on Carbonaceous Sorbents," M.S. Thesis, State University of New York at Buffalo (1982).

Turnock, P. H., and R. H. Kadlec, "Separation of Nitrogen and Methane via Periodic Adsorption," *AIChE J.*, **17**, 335 (1971).

Wang, S. S., "Cyclic Separation of Mixtures of Hydrogen and Methane Using Carbonaceous Sorbents," M.S. Thesis, State University of New York at Buffalo (1982).

Wankat, P. L., J. C. Dore, and W. C. Nelson, "Cycling Zone Separations," *Sep. Purif. Meth.*, **4**, 215 (1975).

Wankat, P. L., "Continuous Recuperative Mode Parametric Pumping," *Chem. Eng. Sci.*, **33**, 723 (1978).

Wong, Y. W., F. B. Hill, and Y. N. I. Chan, "Studies of the Separation of Hydrogen Isotopes by a Pressure Swing Adsorption Process," *Sep. Sci. and Tech.*, **15**, 423 (1980).

Yang, R. T., and R. T. Liu, "Gaseous Diffusion in Porous Solids at Elevated Temperatures," *Ind. Eng. Chem. Fund.*, **21**, 262 (1982).

Manuscript received May 13, 1982; revision received November 2, and accepted January 24, 1983.

One-Dimensional Model of the Physico-Chemical Processes Occurring Inside a Burning Coal Surface

J. G. M. MASSAQUOI and J. B. RIGGS

Department of Chemical Engineering
West Virginia University
Morgantown, WV 26506

A one-dimensional model has been developed to account for the physicochemical processes occurring inside a burning wet coal surface. The model considers the vaporization of coal moisture and the existence of a moving evaporation front, pyrolysis and char/gas reactions in the hot zone, molecular diffusion and Darcy flow through the dry porous coal, transpiration cooling effect of the water vapor and pyrolysis gases, temperature-dependent reaction kinetics and coal thermal conductivity, and variable porosity of the coal due to pyrolysis and char/gas reactions.

The model and associated assumptions have been verified with experimental data from the combustion and drying of coal. The results also show that the model prediction of the heat transferred from the coal surface into the coal is much higher than that calculated by the simple heat conduction equation.

The fraction of the water in the coal that reacts with char is shown as a function of the linear burn velocity and the surface temperature. In addition, the effect of variations in coal moisture and the thermal conductivity on the thickness of the dry zone are also shown.

SCOPE

One of the main problems that arises in modeling of underground coal gasification (UCG) is accounting for the processes occurring between the coal surface and the evaporation front. Most importantly, it is necessary to know how much heat is transferred into the coal, the fraction of coal moisture that reacts with the char and the thickness of this reaction zone. Existing models for simulating UCG have treated the heat transfer in the surrounding seam as a simple pseudosteady-state heat conduction problem (Wong, 1975; Riggs et al., 1979), or, in some cases, arbitrary assumptions about temperature distributions within the coal have been made (Dinsmoor et al., 1978). The possibility of pyrolysis and carbon/steam reactions occurring within the seam is usually ignored and all char/gas reactions are assumed to occur at the cavity wall. A rigorous model of a burning coal surface could be used to assess the relative importance of the various processes occurring in addition to evaluating simplifying assumptions that are used in various coal conversion models.

Figure 1 is a one-dimensional representation of a burning coal surface found during UCG operation. This model is markedly different from coal combustion models used to describe other coal gasification processes. Due to the countercurrent contacting nature of these other coal gasification processes, their combustion zone involves only char gasification. But the combustion zone for a UCG process involves pyrolysis, drying and char gasification, simultaneously. Figure 2 shows the one-dimensional system that is analyzed in this paper. Note that Figure 2 is a subset of Figure 1.

Correspondence concerning this paper must be addressed to J. B. Riggs.